

Exchange Splitting Mechanism of Negative Magnetoresistance in Layered Antiferromagnetic Semimetals

P. D. Grigoriev,^{1,2,3} N. S. Pavlov,⁴ I. A. Nekrasov,⁴ I. R. Shein,⁵ A. V. Sadakov,⁶
O. A. Sobolevskiy,⁶ E. Maltsev,^{7,8} N. Pérez,⁷ L. Veyrat,^{7,8,9} and V. M. Pudalov⁶

¹*L.D. Landau Institute of Theoretical Physics, RAS*

²*National University of Science and Technology "MISiS", 119049, Moscow, Russia*

³*HSE University, Moscow 101000, Russia*

⁴*Institute for Electrophysics, RAS, Ekaterinburg, 620016, Russia*

⁵*Institute of Solid State Chemistry, RAS, Ekaterinburg, 620990, Russia*

⁶*V. L. Ginzburg Research Center at P. N. Lebedev Physical Institute, RAS, Moscow 119991, Russia*

⁷*Leibniz Institute for Solid State and Materials Research, IFW Dresden, D-01069 Dresden, Germany*

⁸*Dresden-Würzburg Cluster of Excellence ct.qmat, Dresden, Germany*

⁹*Laboratoire National des Champs Magnétiques Intenses,
CNRS-INSA-UJF-UPS, F-31400 Toulouse, France*

Layered topologically non-trivial and trivial semimetals with AFM-type ordering of magnetic sublattice are known to exhibit a negative magnetoresistance that is well correlated with AFM magnetization changes in a magnetic field. This effect is reported in several experimental studies with EuFe_2As_2 , EuSn_2As_2 , EuSn_2P_2 , etc., where the resistance decreases quadratically with field by about $\delta\rho/\rho \sim 4 - 6\%$ up to the spin-polarization field. Despite the fact that this effect is well documented experimentally, its theoretical explanation is missing up to date. In this paper we propose novel theoretical mechanism describing the observed magnetoresistance that does not imply either topological origin of the materials, surface roughness, their potential defect structure, or electron-magnon scattering. We believe, the proposed intrinsic mechanism of magnetoresistance is applicable to a wide class of the layered AFM-ordered semimetals. The theoretically calculated magnetoresistance is qualitatively consistent with experimental data for crystals of various composition.

Topology incorporated with magnetism provides a fertile playground for studying novel quantum states and therefore attracts tremendous attention. Topological aspects and related electronic phenomena occurring in antiferromagnetic (AFM) materials are among the central topics in condensed matter physics.

The vast majority of AFM topologically nontrivial insulators (TI) and semimetals (TSM) exhibit such characteristic feature as a negative magnetoresistance (NMR) in a magnetic fields parallel to the basal plane. This effect has recently attracted a great deal of interest, as it is related with chiral anomaly in Dirac and Weyl semimetals [1, 2], with Chern insulators and anomalous quantized Hall state in AFM topological insulators [3, 4]. Indeed, for topological semimetals (Na_3Bi , TaS , Cd_3As_2), a large NMR results from the chiral anomaly [5, 6] and appears only when the electric field is applied nearly parallel to the magnetic field. This NMR is highly anisotropic and its sign changes as the angle between \mathbf{H} and current increases to $\pi/2$ [5]. In the topological insulator (TI) MnBi_2Te_4 , a huge NMR [4] occurs as a result of the topological phase transition from AFM TI to a ferromagnetic Weyl semimetal in external field.

On the other hand, a large number of topologically trivial analogues, the layered AFM semimetals, also exhibit NMR. There is no widely accepted treatment of NMR. Particularly, in doped magnetic materials it is being associated with scattering by magnon and impurities, whereas topology is evidently irrelevant.

In this paper we suggest a novel mechanism of the *in-*

trinsic NMR that is irrelevant to magnons, impurities, and topology and we believe is applicable to a wide class of non-Weyl semimetals, such as EuSn_2As_2 , EuFe_2As_2 , EuSn_2P_2 . We test our model by comparing it with experimentally measured magnetoresistance in EuSn_2As_2 .

This paper focuses on the topologically trivial layered semimetals with AFM-type ordering of the sublattice of magnetic ions. These materials exhibit a negative magnetoresistance that is tightly correlated with the magnetization field dependence. The magnetization changes linearly with external field in conventional manner and sharply saturates above a field of complete spin polarization H_{sf} . The combination of the two closely related effects was reported in several experimental studies with EuFe_2As_2 [7, 8], EuSn_2As_2 , and EuSn_2P_2 [9].

For the particular representative EuSn_2As_2 compound, at $T < 24\text{K}$ the magnetic Eu-sublattice experiences magnetic ordering into the A-type AFM structure in which Eu magnetic moments lie in the easy *ab*-plane and rotate by π from layer to layer along *z*-axis (see Fig. 1a).

Synchronous with magnetization, the diagonal resistivity decreases approximately parabolically with field as $\delta\rho_{xx}(H) \propto -\alpha H^2$. At higher fields $H > H_{\text{sf}}$, magnetotransport perpendicular to the field sharply changes from NMR for a conventional positive magnetoresistance. Such NMR closely correlated with the magnetization $M(H)$ field dependence [7, 9–11] was discussed previously in terms of either nontrivial topological properties, or in terms of scattering by domains, grain boundaries etc., with no detailed theoretical consideration.

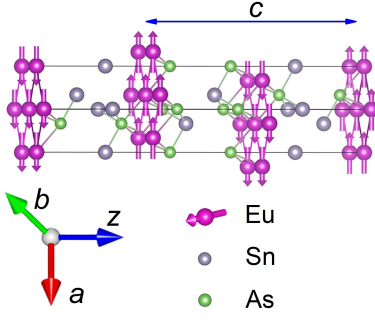


FIG. 1. Schematic picture of the EuSn_2As_2 lattice structure (adapted from Ref. [12]). Magenta arrows show Eu-atoms magnetization direction in the A-type AFM ordered state. Horizontal arrow denotes the lattice spacing $c \approx 2.64\text{nm}$ along z -axis [10, 13, 14].

In this paper we address the issue of the origin of negative parabolic MR. Specifically, (i) we propose a model where NMR universally originates from the enhancement of electron scattering in AFM crystals, (ii) we substantiate this proposal using DFT calculations of the spin polarized charge distribution, and (iii) we compare the model with our experimental data for NMR.

The main idea of the proposed NMR mechanism is as follows. The AFM order violates the \hat{Z}_2 symmetry $1 \leftrightarrow 2$ between two magnetic sublattices (see Fig. 1a). This squeezes the electron wave function $\psi_\sigma(\mathbf{r})$ for each spin component σ and, hence, increases the electron scattering rate [15]

$$1/\tau \propto \int |\psi_\sigma(\mathbf{r})|^4 d^3\mathbf{r} \quad (1)$$

by short-range crystal defects or δ -correlated disorder already in the Born approximation. Figures 2a,b schematically illustrate the violation of \hat{Z}_2 symmetry of the electron wave function by AFM order and the enhancement of $|\psi|^4(\mathbf{r})$ entering the scattering rate in Eq. (1). An external magnetic field \mathbf{H} below the complete spin-polarization and perpendicular to the AFM sublattice magnetization M_{AFM} reduces it approximately according to classical relation [16]

$$\frac{M_{AFM}(H)}{M_{AFM}(0)} \approx \sqrt{1 - \frac{M_H^2}{M_{AFM}^2(0)}} \approx \sqrt{1 - \frac{H^2}{H_{sf}^2}}, \quad (2)$$

where $M_H = \chi H$ is the field-induced magnetization along the magnetic field and perpendicular to AFM order. We took $\chi = \chi_\perp(H) \approx \text{const}$, in agreement with textbook [16] and with experimental data for EuSn_2As_2 [10, 13, 17]. As we show below, the degree of \hat{Z}_2 symmetry violation and $1/\tau$ enhancement depends on the ratio

$$\gamma = \Delta E_{ex}/2t_0 \quad (3)$$

of the exchange splitting ΔE_{ex} of conduction electron bands to their hopping amplitude t_0 between the opposite

AFM sublattices (Fig. 1a). While t_0 is determined by the band structure and does not considerably depend on H , the exchange splitting $\Delta E_{ex} \propto M_{AFM}(H)$ decreases with H according to Eq. (2):

$$\frac{\Delta E_{ex}(H)}{\Delta E_{ex}(H=0)} = \frac{M_{AFM}(H)}{M_{AFM}(0)} \approx \sqrt{1 - (H/H_{sf})^2}. \quad (4)$$

This leads to a parabolic negative magnetoresistance almost up to the field H_{sf} . Closer to the spin polarization transition, at $H \rightarrow H_{sf}$ a first-order spin-flip phase transition causes a much faster decrease of $M_{AFM}(H)$ than that given by Eq. (2).

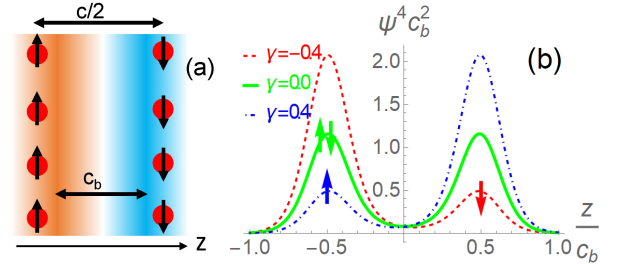


FIG. 2. Wave functions magnitude distribution along the crystal z -axis, for the lowest-energy quantum state [Eq. (7)] in a double-well potential, modeling two AFM sublattices. (a) Schematic color illustration of the spin-up (red) and spin-down (blue) wave function distribution along the z -axis in the half-cell of the $c/2$ -size. c_b denotes the distance between the two spin-split WF maxima. Color intensity represents the WF magnitude. Circles show Eu-atoms, and arrows - their magnetization direction in the AFM state. (b) Schematic picture of the fourth power $\psi^4(z)$, entering the scattering rate in Eq. (1). The asymmetry parameter is $\gamma \equiv \Delta E_{Zex}/2t_0 = 0$ (green solid line), $\gamma = -0.4$ (dashed red line) and $\gamma = 0.4$ (dash-dotted blue line).

Let us consider the electron wave functions squeezing in the AFM state. The two AFM sublattices are numerated by the index $i = 1, 2$ or by the "pseudospin" $\lambda = \lambda(i) = 3/2 - i$, while the projection of spin on the magnetization axis \mathbf{M}_{AFM} is denoted by $\sigma = \pm 1 \equiv \uparrow, \downarrow$. The quantum basis consists of four states, $|i, \sigma\rangle = \{1 \uparrow, 1 \downarrow, 2 \uparrow, 2 \downarrow\}$, corresponding to wave functions $\psi_{i,\sigma} = \{\psi_{1\uparrow}, \psi_{1\downarrow}, \psi_{2\uparrow}, \psi_{2\downarrow}\}$. The usual Zeeman splitting $\Delta E_Z(\mathbf{H}) = (\vec{\sigma} \cdot \vec{H}) g\mu_H/2$ in a relevant external magnetic field $H \lesssim 5\text{T}$ is much smaller than the exchange splitting $\Delta E_{ex} \gtrsim 10\text{meV}$ and will be neglected below. Then the AFM-sublattice part of the electron Hamiltonian for each electron quasi-momentum \mathbf{k} is given by the 4×4 matrix, which decouples into two 2×2 matrices:

$$\hat{H}_\sigma = \begin{pmatrix} \Delta E_{ex}\sigma/2 & t_0 \\ t_0^* & -\Delta E_{ex}\sigma/2 \end{pmatrix}. \quad (5)$$

Here the non-diagonal term $t_0 = t_0^*$ is the intersublattice electron transfer integral. The diagonalization of Hamil-

tonian (5) gives two eigenvalues

$$E_{\pm,\sigma} = \mp \sqrt{\Delta E_{ex}^2/4 + t_0^2} \quad (6)$$

and the corresponding wave functions (WF)

$$\psi_{\pm,\sigma} = \frac{\psi_1 \left(\sigma\gamma \pm \sqrt{\gamma^2 + 1} \right) + \psi_2}{\sqrt{1 + \left(\sigma\gamma \pm \sqrt{\gamma^2 + 1} \right)^2}}, \quad (7)$$

where $\psi_{1,2}$ are the electron wave functions “localized” mostly on the first and second AFM sublattices. Without the AFM order, i.e. at $\Delta E_{ex} = 0$, one gets the electron spectrum $E_{\pm,\sigma} = \mp t_0$ and the corresponding normalized eigenstates

$$\psi_{\pm,\sigma}^s = (\psi_1 \pm \psi_2) / \sqrt{2}, \quad (8)$$

which are symmetric and antisymmetric superpositions of electron states on sublattices 1 and 2, as it should be when the \hat{Z}_2 symmetry is conserved. From Eqs. (7) we see that AFM lifts this symmetry, making the eigenfunction amplitude larger on one of two sublattices, as illustrated in Fig. 2. This enhances the integral in Eq. (1), as seen from Figs. 2 and shown below.

In the Born approximation, i.e. the second-order perturbation theory in the impurity potential, the electron scattering rate is given by the Fermi’s golden rule [15]:

$$\frac{1}{\tau} = \frac{2\pi}{\hbar} \sum_{n',i} \left| T_{n'\mathbf{n}}^{(i)} \right|^2 \delta(\varepsilon_{\mathbf{n}} - \varepsilon_{\mathbf{n}'}). \quad (9)$$

where the index $n \equiv \{\mathbf{k}, \zeta, \sigma\}$ numerates quantum states, ζ and σ denote the electron subband and spin projection, $\varepsilon_{\mathbf{n}}$ is the electron energy in state n , and $\delta(x)$ is the Dirac delta-function. The short-range impurities or other crystal defects in solids are, usually, approximated by the point-like potential $V_i(\mathbf{r}) = U\delta(\mathbf{r} - \mathbf{r}_i)$. Here we omit the spin index σ because it is conserved by the potential scattering. The corresponding matrix element of electron scattering by this impurity potential is $T_{n'\mathbf{n}}^{(i)} = U\Psi_{n'}^*(\mathbf{r}_i)\Psi_{\mathbf{n}}(\mathbf{r}_i)$, where $\Psi_{\mathbf{n}}(\mathbf{r})$ is the electron wave function in the state \mathbf{n} .

For short-range impurities the matrix element does not depend on electron momentum \mathbf{k}' . Then the summation over \mathbf{k}' with the δ -function in Eq. (9) gives the electron density of states (DoS) $\nu_{F\zeta} \equiv \nu_{\zeta}(\varepsilon_F)$ at energy Fermi ε_F per one spin component and per one subband ζ . The total DoS per one spin $\nu_F = \sum_{\zeta} \nu_{F\zeta}$. If the impurities are uniformly and randomly distributed in space, the sum over impurities rewrites as an integral over impurity coordinate: $\sum_i \rightarrow n_i \int d^3\mathbf{r}_i$, where n_i is the impurity concentration. Then Eq. (9) becomes

$$\frac{1}{\tau} = \frac{2\pi}{\hbar} n_i U^2 \int d^3\mathbf{r}_i \sum_{\zeta'} \nu_{F\zeta'} |\Psi_{\mathbf{k}'\zeta'}^*(\mathbf{r}_i)\Psi_{\mathbf{k}\zeta}(\mathbf{r}_i)|^2. \quad (10)$$

The Bloch wave function is $\Psi_{\mathbf{k}\zeta}(\mathbf{r}) = \psi_{\zeta}(\mathbf{r}) \exp(i\mathbf{k}\mathbf{r})$, where $\psi_{\zeta}(\mathbf{r})$ is the periodic function. Then Eq. (10) rewrites as

$$\frac{1}{\tau} = \frac{2\pi}{\hbar} n_i U^2 \nu_F I, \quad (11)$$

where the integral over one elementary cell

$$I \equiv \int d^3\mathbf{r} |\psi_{\zeta}(\mathbf{r})|^2 \sum_{\zeta'} \frac{\nu_{F\zeta'}}{\nu_F} |\psi_{\zeta'}(\mathbf{r})|^2. \quad (12)$$

For a single band ζ at the Fermi level, i.e. when $\nu_{F\zeta'} = 0$ for $\zeta' \neq \zeta$, this confirms Eq. (1). Eqs. (11) and (12) also result to Eq. (1) if only the scattering within the same band is allowed, e.g., due to the spin conservation during the potential scattering. Eqs. (11),(12) approximately give Eq. (1) also when there are several bands, but the DoS $\nu_{F\zeta}$ for one band ζ is much larger than that for the others. The latter happens in Dirac semimetals, where the DoS $\nu_{\zeta}(\varepsilon_F) \propto \varepsilon_F^{d-1}$ strongly depends on the Fermi energy ε_F and where the energy difference $\varepsilon_{\zeta'}(\mathbf{k}) - \varepsilon_{\zeta}(\mathbf{k}) \gtrsim \varepsilon_F$ for $\zeta' \neq \zeta$.

Now we estimate the difference δI of two integrals (12) for the asymmetric and symmetric wave functions, given by Eqs. (7) and (8). The host crystal lattice has the \hat{Z}_2 symmetry, therefore $\int \psi_1^4(z) dz = \int \psi_2^4(z) dz$. For simplicity, we also assume that the overlap of the wave functions on different AFM sublattices is negligible, i.e. $\psi_1\psi_2 \ll |\psi_1|^2$, and we neglect the products $\psi_1\psi_2 \approx 0$. The main conclusion remains valid also when $\psi_1\psi_2 \sim |\psi_1|^2$, but the calculation are more cumbersome.

First we consider the completely subband-polarized case $\nu_{F\zeta}/\nu_F = 1$ for $\zeta = 1$ and $\nu_{F\zeta}/\nu_F = 0$ for $\zeta = 2$. Then for the symmetric wave function (8), corresponding to the lowest subband ζ without the AFM order and bilayer asymmetry, the integral (12) is

$$I_0 = \int d^3\mathbf{r} |\psi_+^s|^4 dz \approx \int d^3\mathbf{r} \psi_1^4/2. \quad (13)$$

We now calculate the difference

$$\delta I \equiv I - I_0 = \int d^3\mathbf{r} \left(|\psi_+|^4 - |\psi_+^s|^4 \right), \quad (14)$$

which gives the correction to mean free time τ according to Eq. (1) or (11). After the substitution of Eqs. (7) and (8), at $\psi_1\psi_2 \ll |\psi_1|^2$ this simplifies to

$$\delta I \approx \frac{\gamma^2}{1 + \gamma^2} \int d^3\mathbf{r} \frac{\psi_1^4(z)}{2} = \frac{\gamma^2 I_0}{1 + \gamma^2} = \frac{\gamma^2 I}{1 + 2\gamma^2}. \quad (15)$$

At $\gamma^2 \ll 1$ Eq. (15) simplifies to $\delta I \approx \gamma^2 I_0 \approx \gamma^2 I$, and substituting Eqs. (15), (3) and (4) to (11) we obtain the relative increase of resistivity due to the AFM ordering

$$\frac{\delta\rho(H)}{\rho(0)} \approx \frac{\delta I}{I} \approx \frac{[\delta(H)]^2}{1 + 2[\delta(H)]^2} \approx \left(\frac{\Delta E_{ex}}{2t_0} \right)^2 \left(1 - \frac{H^2}{H_{sf}^2} \right). \quad (16)$$

Contrary to the NMR caused by chiral anomaly in Weyl semimetals, this increase of resistivity is *isotropic*. For example, our NMR mechanism applies both for the interlayer and in-plane current directions in layered conductors, and it only slightly depends on the magnetic field direction due to a magnetic anisotropy solely.

At $H > H_{\text{sf}}$ the obtained correction (16) disappears, and one returns to the usual positive magnetoresistance in multiband conductors due to impurity scattering, which is parabolic at low field when $\omega_c\tau \ll 1$ [14]:

$$\rho_{zz}^m(H)/\rho_{zz}^m(0) = 1 + \omega_c^2\tau^2, \quad \omega_c\tau \ll 1, \quad (17)$$

where $\omega_c = eH/(m^*c)$ is the cyclotron frequency. Combining Eqs. (16) and (17) gives the schematic MR curve

$$\frac{\rho(H)}{\rho(0)} \approx 1 - \frac{(\Delta E_{ex}/2t_0)^2}{1 + 2(\Delta E_{ex}/2t_0)^2} \frac{H^2}{H_{\text{sf}}^2} + [\omega_c(H)\tau]^2, \quad (18)$$

illustrated in Fig. 3a, which resembles very much the experimental observations shown in Fig. 4. The first-order spin-flip phase transition leads to a jump or much faster decrease of AFM order parameter $M_{\text{AFM}}(H)$ at $H \approx H_{\text{sf}}$ than the continuous dependence given by Eq. (2). Hence, at H close to spin-polarization field H_{sf} the resistivity drops faster than in Eqs. (16), (18), or in Fig. 3a.

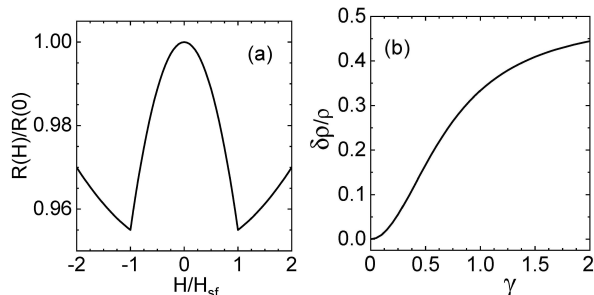


FIG. 3. (a) Magnetoresistance curve given by Eq. (18) at $\Delta E_{Zex}/2t_z = 0.1$ and $[\omega_c\tau(H = H_{\text{sf}})]^2 = 0.2$. (b) The maximal possible relative value of the proposed NMR effect as a function of $\gamma = \Delta E_{ex}/2t_0$, plotted using Eqs. (15) or (16). It saturates to 50% at $\gamma \gg 1$, when resistivity drops by half.

In usual 3D AFM metals the proposed NMR mechanism is very weak, because the ratio $\gamma = \Delta E_{ex}/2t_0 \ll 1$. Indeed, $\Delta E_{ex} \lesssim 0.1\text{eV}$, while $2t_0 \sim 1\text{eV}$ is comparable to the bandwidth. However, in strongly anisotropic layered materials with A-type AFM order the ratio $\gamma = \Delta E_{ex}/2t_0 \sim 1$, because the interlayer transfer integral $t_0 \lesssim 0.1\text{eV}$ in van-der-Waals or other layered compounds is also small.

Comparison of the model with experimental data. To compare the presented theory with experimental data, we performed magnetization and magnetoresistance measurements with EuSn_2As_2 bulk single crystals.

The normalized $R(H)/R(0)$ magnetoresistance and magnetization $M(H)$ dependences are shown in Fig. 4

for two field orientations $H\|c$ and $H\|ab$ at low temperature $T \approx 2\text{K}$, $T \ll T_N \approx 24\text{K}$. The most striking here is the NMR hump that is the focus of our study. NMR terminates sharply at the full spin polarization field H_{sf} , and the hump magnitude is roughly the same for $H\|c$ and $H\|ab$.

For the majority of samples, NMR indeed varies about quadratically with field as Fig. 4 shows. Whereas the NMR magnitude is about the same for all studied samples, in low fields NMR looks somewhat more flattened. Scaling analysis of the “flattened” NMR [14] reveals that it may be decomposed into two terms. Besides the main *negative* parabolic term that extends to H_{sf} , there is a minor *positive* term that starts parabolically from $H = 0$ and then disappears as field increases, already at $H \approx 2 - 3T < H_{\text{sf}}$. Its possible origin is discussed further. We therefore consider the quadratic-type NMR (see Fig. 4) to be generic dependence (NQMR) and compare it with theory.

As field increases and exceeds H_{sf} , the NQMR hump changes sharply to the conventional smooth parabolic rise. We highlight that the sharp transition between the negative (NQMR) and positive (PMR) magnetoresistance (i.e. the $R(H)$ minima) coincides with the sharp magnetization saturation at $H = H_{\text{sf}}$ for both field directions (Figs. 4a,b). This is consistent also with previous studies [10, 11, 18]. Comparing this data with the presented first-order in $(\omega_c\tau)^2$ model, we conclude that the model correctly captures the main features: approximately parabolic NMR, its magnitude, and a sharp transition to the conventional PMR.

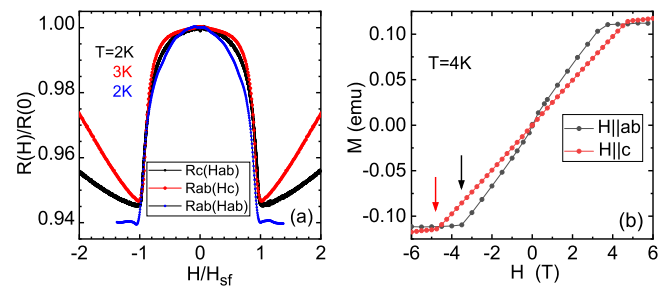


FIG. 4. (a) Examples of the normalized magnetoresistance $R(H)/R(0)$ vs normalized field (H/H_{sf}) for two orientations of the bias current, in-plane R_{ab} and perpendicular to the plane R_c , and for two magnetic field directions, $H\|(ab)$ and $H\|c$. Data are taken at $T = 2 - 3\text{K}$. (b) Magnetization $M(H)$ dependences for two field orientations, $\mathbf{H}\|ab$ and $\mathbf{H}\|c$. The nonlinearity of $M(H\|ab)$ in low fields is related with spin canting and spin-flop [14]. Vertical arrows depict the complete spin polarization field H_{sf} .

In our measurements on EuSn_2As_2 crystals with A-type AFM order, the magnetoresistance $\delta\rho/\rho$ drops by about 5 – 6%, as shown in Fig. 4. According to Eqs. (16) and (3) for the band-polarized case $\Delta E_{\zeta} > \varepsilon_F$ this NQMR drop corresponds to

$$\Delta E_{ex}/4t_0 = \sqrt{\delta\rho/4\rho} \approx 0.11. \quad (19)$$

We now compare this ratio with our DFT calculations and ARPES data for ΔE_{ex} and $4t_0$. From the DFT calculations we found $\Delta E_{ex} \approx 30$ meV level splitting for EuSn_2As_2 [14]. Substituting this to Eq. (19) one gets $t_0 \approx 67$ meV. The ARPES data [14, 19] do not have sufficient energy resolution to measure the bilayer splitting and t_0 directly. However, the t_0 value can also be roughly estimated from the observed resistivity anisotropy $\rho_{zz}/\rho_{xx} \approx 100$ [14] and the width of the in-plane energy band $4t_x \approx 1.9$ eV, which is taken from our ARPES data and from the DFT calculation. As a result, we obtain the lowest estimate $t_0 \approx t_x \sqrt{\rho_{xx}/\rho_{zz}} \approx 50$ meV, which is in a reasonable agreement with $t_0 \approx 67$ meV determined from Eq. (19).

Now we check whether our assumption of complete polarization is valid for EuSn_2As_2 . The DFT calculations and ARPES data for EuSn_2As_2 give rather small Fermi energies ε_F for all Fermi-surface pockets [14]. According to the DFT calculations, there are two electron bands with $\varepsilon_F \approx 55$ meV and $\varepsilon_F \approx 100$ meV and two hole bands with $\varepsilon_F \approx 65$ meV and $\varepsilon_F \approx 80$ meV. In order to test whether our assumption of the complete band polarization is applicable to EuSn_2As_2 , these Fermi energies must be compared with the band splitting

$$\Delta E_\zeta = E_- - E_+ = 2\sqrt{\Delta E_{ex}^2/4 + t_0^2}. \quad (20)$$

Substituting $t_0 \approx t_{z0\rho} \approx 50$ meV and $\Delta E_{ex} \approx 30$ meV to Eq. (20) we get the band splitting $\Delta E_\zeta \gtrsim 100$ meV $> \varepsilon_F$ for all Fermi-surface pockets. We conclude, EuSn_2As_2 corresponds to the completely band-polarized case for all electronic bands at the Fermi levels, and the above analysis, including Eq. (16), is applicable to the experimental data for EuSn_2As_2 .

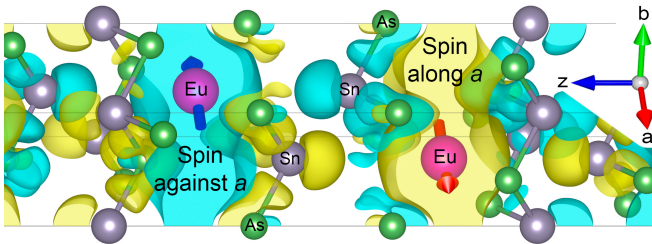


FIG. 5. Calculated spin-polarized electron density distribution. The yellow (turquoise) isosurfaces correspond to fixed differences of charge density with spin along (against) the a axis of AFM ordering of Eu spins. The neighboring SnAs layers have opposite spin polarization of electrons at the Fermi level thus substantiating our model.

To substantiate our model of opposite spin polarization of conducting electrons on neighboring SnAs layers we performed the ab-initio calculation of spin-polarized electron density distribution using the density-functional theory (DFT). Our results are shown in Fig. 5, where the yellow (turquoise) isosurfaces limit the real-space areas filled with the same color of positive (negative) electron spin density exceeding a fixed absolute value. As

we assumed in our model and illustrated in Fig. 2, the neighboring SnAs layers indeed have opposite spin polarization of conducting electrons. This spin polarization in EuSn_2As_2 is small, $\sim 0.1\%$ of total electron density, but it is peaked at the Fermi level and strongly affects the electron scattering rate according to the above analysis.

We highlight that the proposed NMR mechanism also applies to multiband conductors, where at least one band is completely polarized, or even to those where at the Fermi level the DoS for two subbands splitted by ΔE_ζ differ considerably. However, if all bands are polarized, the described NMR effect becomes stronger and may approach its theoretical limit of 50% at $\gamma \gg 1$, shown in Fig. 3b, when the resistivity drops by half.

Discussion

We assess below the potential influence of other possible mechanisms on NMR in layered AFM semimetals.

(i) Electron-magnon scattering. For antiferromagnets, MR was found to be *positive* [20–22], and for $T \ll T_N$ to increase quadratically with field. The magnetoresistance originates from a field-induced increase in spin fluctuations. This theoretical result is confirmed by a large number of experimental studies, e.g. on antiferromagnetic Mn_2Au [23] and PrB_6 [24].

Probably, this mechanism is responsible for a minor flattening of NQMR in low fields, that is observed for the studied EuSn_2As_2 samples (see Fig. 4a). Indeed, adapting the results of Refs. [20, 21] to our case of the easy-plane antiferromagnet [22] we anticipate: $\Delta\rho(H)/\rho(0) \propto (\mu_B H_{c1}/T)^2 (H/H_{c1})^2$ for $\mathbf{H}\parallel ab$, and $\Delta\rho(H)/\rho(0) \propto (T/T_N)^2 (H/H_{c2})^2$ for $\mathbf{H}\parallel c$. Here H_{c1} is the spin-flop field, and $H_{c2} = H_{sf} \sim 5$ T. Since H_{sf} is much larger than H_{c1} , it follows, that for the $\mathbf{H}\parallel c$ orientation PMR should extend to much higher fields $\sim H_{sf}$ and to raise with temperature. For the $\mathbf{H}\parallel ab$ orientation, PMR is pronounced only in low fields $\sim H_{c1}$ and decays with increasing T . This behavior is qualitatively consistent with flattening of the measured $R(H)$ dependences shown in Fig. 4 for various field orientations. The magnon scattering might also contribute to the transformation with temperature raising of NQMR to a positive magnetoresistance (for more detail, see [14]).

In contrast, for ferromagnets the magnetoresistance related with magnon scattering is negative and originates from the magnetic-field-induced suppression of scattering. This type of low temperature NMR was reported for ferromagnetic DyNiBC , GdNiBC , HoNiBC , and TbNiBC [25]. We note that the studied in our work EuSn_2As_2 compound is stoichiometric, antiferromagnetic in the low temperature range of interest (on a large mesoscopic scale $> \lambda_F$), and has no FM impurities.

(ii) Kondo-scattering, i.e. the scattering of conduction electrons due to randomly located magnetic impurities. This scattering results in a characteristic minimum in electrical resistivity with temperature. In our case, firstly, no such a minimum or even a tendency is observed [14], and secondly, there are no magnetic impurities in the stoichiometric EuSn_2As_2 compound grown

from high purity raw materials.

(iii) In ferromagnetic oxides, such as $\text{Ln}_{1-x}\text{Ca}_x\text{MnO}_3$, the magnetoresistance is negative and also correlates with magnetization [26]: the magnetoresistance in this case is phenomenologically described as $R(H, T) \propto \exp[-M(H, T)/M_0]$ and is explained by polaronic hopping transport below the ferromagnetic ordering temperature T_c . The model of polaron hopping transport in insulating oxides is evidently inapplicable to the semimetallic and well conducting EuSn_2As_2 characterized by the diffusive- rather than hopping-type transport.

(iv) Giant magnetoresistance (GMR). The observed NQMR, at first glance, is reminiscent of GMR in superlattices of Fe/Cr where resistance decreases as magnetization in the neighbouring Fe-layers turns with external field from antiparallel to parallel [27]. However, GMR is known to develop for charge transport across the layers, while NQMR under study is fully isotropic.

(v) The chiral anomaly and nontrivial topology are often considered as the origin of the NQMR, e.g. in EuIn_2As_2 and MnBi_2Te_4 . Regarding the investigated compound EuSn_2As_2 , our ARPES measurements [14] didn't reveal band crossings and Dirac points in the close vicinity of the Fermi level. The magnetotransport measurements also showed that $\delta R(H)/R(H)$ is almost independent (within 10%) of the field direction $H\parallel ab$ or $H\parallel c$, of the charge transport direction, in-plane $R_{ab}(H)$ or normal to the plane $R_c(H)$ (see Fig. 4 and also [14]). NQMR is also independent of the angle between the electric and magnetic field in the easy ab -plane [14]. These results exclude topological origin of NQMR in EuSn_2As_2 . The independence of NQMR on the sample thickness (from 60 nm to 0.2 mm) [28] indicates that NQMR does not come from scattering by large-scale macroscopic lattice defects (such as misfit dislocations, domains, misoriented grains) and the sample ab -plane bending, since these imperfections are expected to be different for the bulk crystal and for exfoliated flakes a few monolayer thick.

Summarizing the above brief review, we conclude that the previously known and discussed mechanisms cannot explain the observed NQMR in the layered topologically trivial AFM semimetals. Nevertheless, we believe that the flattening of NMR in low fields may be caused by the positive MR contribution from electron-magnon scattering.

The approximately quadratic negative magnetoresistance measured in this work is similar to that observed earlier in other studies with EuSn_2As_2 [11, 18], and with sister materials – EuFe_2As_2 [7], and EuSn_2P_2 [9]. We, therefore, believe that our model is applicable to the listed materials. The similarity in NMR also indicates insignificance of such features as the existence of Dirac states close to E_F in EuSn_2P_2 [9], a stripe SDW in the Fe

chains and a more complex biquadratic coupling between Eu- and Fe-atoms in EuFe_2As_2 .

There are other more complex behaviors of magnetoresistance in more complex layered materials, for example, in ferromagnetic Weyl semimetal EuCd_2As_2 [29], in axion insulator EuIn_2As_2 [2, 30], and AFM topological insulators EuMg_2Bi_2 [31], MnBi_2Te_4 and MnBi_4Te_7 [32, 33]. Obviously, these cases are beyond the framework of the considered model.

The proposed model helps to extract useful information about the electronic structure of AFM compounds from measurements of the NQMR effect. Indeed, according to Eqs. (16) or (18), the NQMR magnitude gives the parameter $\gamma = \Delta E_{ex}/2t_0$, i.e. the ratio of exchange energy splitting to the hopping amplitude between AFM sublattices. The sharp NQMR-minimum also helps determine the magnetic field H_{sf} of complete spin polarization without magnetization measurements.

To conclude, we clarified the origin of the *negative parabolic* magnetoresistance observed in layered AFM semimetals. Specifically, we suggested a novel type of magnetoresistance mechanism and developed a theory describing parabolic NMR over a wide field range up to complete spin polarization. In the proposed theory, the negative magnetoresistance originates from the violation of \hat{Z}_2 symmetry and the corresponding stronger localization of electron wave functions on one of the two AFM sublattices depending on electron spin. In the analyzed semimetals these AFM sublattices are oppositely polarized layers of magnetic ions in the host lattice. The proposed mechanism of the parabolic NMR is generic for the layered AFM van-der-Waals semimetals; its strength increases as the ratio of the exchange splitting to the transfer integral increases.

The proposed model agrees qualitatively with the available data for layered AFM semimetals, such as EuSn_2As_2 , EuFe_2As_2 , EuSn_2P_2 . This agreement is a strong evidence that NMR in the layered AFM semimetals is an intrinsic property, irrelevant to defects, domains, and other sample-specific disorder.

Acknowledgements. AVS, OAS, and VMP were supported within State Assignment of the research at LPI. PDG acknowledges State Assignment # FFWR-2024-0015, NUST “MISIS” Grant # K2-2022-025 and “Basis” Foundation for Grant # 22-1-1-24-1. NSP, IAN and IRS acknowledge partial support of the State Assignment # 124022200005-2 of Institute of Electrophysics and # 124020600024-5 of Institute of Solid State Chemistry UB RAS. AVS, OAS, VMP, NSP and IAN acknowledge support from RSCF (grant # 23-12-00307). LV acknowledges support from the Leibniz Gemeinschaft through the Leibniz Competition. Experimental work was partly done using equipment of LPI Shared facility Center.

[1] H. Li, H. He, H.-Z. Lu, H. Zhang, H. Liu, R. Ma, Z. Fan, S.-Q. Shen, and J. Wang, Nat. Commun. **7**, 10301

(2015). DOI: 10.1038/ncomms10301.

- [2] J. Yan, Z. Z. Jiang, R. C. Xiao, W. J. Lu, W. H. Song, X. B. Zhu, X. Luo, Y. P. Sun, and M. Yamashita Phys. Rev. Research **4**, 013163 (2022).
- [3] Jiaheng Li, Chong Wang, Zetao Zhang, Bing-Lin Gu, Wenhui Duan, and Yong Xu, Phys. Rev. B **100**, 121103(R) (2019).
- [4] J. Ge, Y. Liu, J. Li, et al. Natl. Sci. Rev. **7**, 1280 (2020).
- [5] Jun Xiong et al., Science **350**, 413 (2015). DOI:10.1126/science.aac6089
- [6] X. Huang, L. Zhao, Y. Long, et al., Phys. Rev. X **5**, 031023 (2015).
- [7] Shuai Jiang, Yongkang Luo, Zhi Ren, et al. New J of Phys **11**, 025007 (2009).
- [8] Joshua J. Sanchez et al., Phys. Rev. B **104**, 104413 (2021).
- [9] Xin Gui, Ivo Pletikoscic, Huibo Cao, et al., ACS Centr. Sci. **5**(5), 900 (2019). doi: 10.1021/acscentsci.9b00202
- [10] Huan-Cheng Chen et al., Chin. Phys. Lett. **37**, No. 4, 047201 (2020).
- [11] H. Li, W. Gao, Z. Chen et al., Phys. Rev. B **104**, 054435 (2021)
- [12] I. A. Golovchanskiy, N. N. Abramov, V. A. Vlasenko, et al. Phys. Rev. B, **106**, 024412 (2022).
- [13] M. Q. Arguilla, N. D. Cultrara, Z. J. Baum, S. Jiang, R. D. Ross and J. E. Goldberger et al., Inorg. Chem.Front **4**, 378 (2017).
- [14] K.S. Pervakov, A.V. Sadakov, O.A. Sobolevskiy, V.A. Vlasenko, V.P. Martovitsky, E.I. Maltsev, N. Pérez, L. Veyrat, P.D. Grigoriev, N.S. Pavlov, I.A. Nekrasov, O.E. Tereshchenko, V.A. Golyashov, and V. M. Pudalov, to be published elsewhere.
- [15] A. A. Abrikosov, *Fundamentals of the theory of metals*, North-Holland, 1988.
- [16] C. Kittel, *Quantum theory of Solids*, J. Wiley & Sons, Inc. 1963.
- [17] S. Pakhira, T. Heitmann, S. X. M. Riberolles, B. G. Ueland, R. J. McQueeney, D. C. Johnston, and David Vaknin, Phys. Rev. B **103**, 024408 (2021).
- [18] Hualei Sun et al., Sci. China, **64**, No. 11: 118211 (2021).
- [19] Hang Li et al., Phys. Rev. X **9**, 041039 (2019).
- [20] H. Yamada, and Satoshi Takada, J. Phys. Soc. Jpn., **34**, 51 (1973).
- [21] H. Yamada, and Satoshi Takada, Progress of Theor. Phys, **49**, 1401 (1973).
- [22] We presume that for our case of the easy magnetization ab plane, the $\mathbf{H}\parallel ab$ and $\mathbf{H}\parallel c$ field orientations correspond in notations of Ref. [21] to the easy axis $\mathbf{H}\parallel z$, and perpendicular to it $\mathbf{H}\parallel x$, respectively.
- [23] S. Yu. Bodnar, Y. Skourski, O. Gomonay, J. Sinova, M. Kläui, and M. Jourdan, Phys. Rev. Applied, **14**, 014004 (2020).
- [24] Naushad Ali, S. So Woods, J. Appl. Phys. **61**, 4393 (1987).
- [25] M. B. Fontes, J. C. Trochez, B. Giordanengo, S. L. Bud'ko, D. R. Sanchez, and E. M. Baggio-Saitovitch, Phys. Rev. B **60**, 6781 (1999).
- [26] M. F. Hundley, M. Hawley, R. H. Heffner, et al., Appl. Phys. Lett. **67**, 860 (1995).
- [27] M. N. Baibich, J. M. Broto, A. Fert et al., Phys. Rev. Lett. **61**, 2472 (1988).
- [28] E. I. Maltsev, L. Veyrat, N. R. Perez, R. Giraud, J. Dufouleur, and B. Büchner, K. S. Pervakov and V. M. Pudalov, to be published elsewhere.
- [29] S. Roychowdhury, M. Yao, K. Samanta, D. Chen, N. Kumar, S. N. Guin, H. Borrmann, M. G. Vergniory, C. Shekhar, C. Felser, Adv. Sci. **10**, 2207121 (2023).
- [30] F. H. Yu, H. M. Mu, W. Z. Zhuo, et al. Phys. Rev. B **102**, 180404(R) (2020).
- [31] M. Marshall, I. Pletikosić, M. Yahyavi, H.-Ju Tien, T.-R. Chang, H. Cao, W. Xie1, J. Appl. Phys. **129**, 035106 (2021).
- [32] J. Ge, Y. Liu, J. Li, et al. Natl. Sci. Rev. **7**, 1280 (2020).
- [33] A. Tan, V. Labracherie, N. Kunchur, A. U. B. Wolter, J. Cornejo, J. Dufouleur, B. Büchner, A. Isaeva, and R. Giraud, Phys. Rev. Lett. **124**, 197201 (2020).